ACS Catalysis

pubs.acs.org/acscatalysis

Research Article

Impact of Nonzeolite-Catalyzed Formation of Formaldehyde on the Methanol-to-Hydrocarbons Conversion

Vladimir Paunović,* Patrick Hemberger, Andras Bodi, Roland Hauert, and Jeroen A. van Bokhoven

Cite This: *ACS Catal.* 2022, 12, 13426−13434

Read Online

ACCESS | Metrics & More | Article Recommendations | Supporting Information

ABSTRACT: Formaldehyde is an important intermediate that affects the catalyst performance in the methanol-to-hydrocarbons (MTH) conversion. In this study, photoelectron photoion coincidence spectroscopy was applied to elucidate the formation of this species in empty quartz and stainless steel reactors as well as over zeolite catalysts (ZSM-5 and BETA) and commonly used bed diluents (silicon carbide and quartz). The yields of formaldehyde in an empty stainless steel reactor and over the crude silicon carbide particles were found to be higher or comparable to those over the zeolite catalysts under similar reaction conditions. In the former two systems, formaldehyde is formed via methanol dehydrogenation, which is catalyzed by transition metals and yields hydrogen and carbon monoxide as the main byproducts. Thus produced formaldehyde is readily consumed in the MTH reaction, wherein its conversion is higher for the more acidic zeolites. The formaldehyde generated by the transition metal sites causes a decrease of the catalyst stability as well as a reduction of the propene-to-ethene ratio, as corroborated by catalytic tests exploring different contacting patterns between the ZSM-5 catalyst and stainless steel chips or silicon carbide particles. These results uncover an important role of methanol dehydrogenation in the MTH conversion, which is relevant for the laboratory testing of the zeolite catalysts and the industrial implementation of this technology.

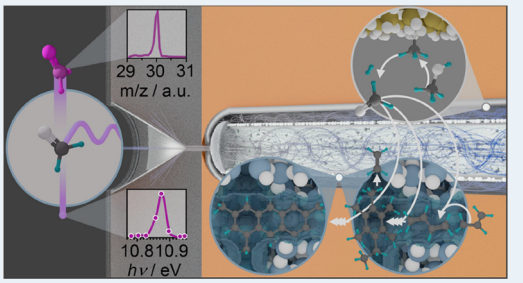

KEYWORDS: *catalyst deactivation, formaldehyde, photoelectron photoion coincidence spectroscopy, wall effects, zeolites*

1. INTRODUCTION

Methanol-to-hydrocarbons (MTH) conversion over microporous solid acid catalysts enables the production of the world's most needed petrochemicals and liquid fuels from nonpetroleum-based feedstock including potentially renewable resources.[1−3] After the initial build-up of the first C_{2+} species, the MTH transformation proceeds through a sequence of alkylation and cracking reactions of the alkene- and arene-based hydrocarbon pool (HP) intermediates, which are interconverted via dealkylation, cyclization, and hydrogen transfer (HT) reactions.[1−5] Therein, the alkene HP mediates the formation of propene and higher alkenes, while the arene HP yields ethene, propene, methylated benzenes, and naphthalenes.[1,3] Nonetheless, the MTH reactions also yield heavier byproducts, primarily alkylated polycyclic aromatic hydrocarbons (PAHs), which progressively accumulate in the form of coke deposits, thus diminishing the micropore volume and precluding the transfer of reactants and products.[6−9] Catalyst coking is the central roadblock in the MTH transformation as it provokes productivity decay and introduces the need for high-temperature reactivation, which wastefully burns a part of feed converted to coke and induces degradation of zeolite.[6−8,10−12]

It is widely accepted that PAHs grow through overalkylation and condensation of the arene HP species.[6,7] These processes proceed primarily via HT, comprising protonation and subsequent hydride transfer.[4,13−15] In the latter bimolecular step, hydride is transferred to surface-activated alkyl or carbenium ions from an aliphatic hydrocarbon or methanol. The hydride acceptors are thus transformed to more saturated (cyclo)alkanes, and the hydride donors, that is, unsaturated hydrocarbons and methanol, are converted to polyenes and formaldehyde, respectively.[13] While polyenes are well-known precursors of the arene HP, formaldehyde was recently pinpointed as a highly potent species in the reaction cascades leading to the synthesis of the first C−C bond, arene HP, and PAH molecules.[6,7,13,16−24] HT pathways involving methanol disproportionation and its reactions with alkenes are inferred as the main sources of formaldehyde in the MTH transformation.[13,15,21,25,26] They are catalyzed by Brønsted acid sites (BAS), while HT from methanol to alkenes can be additionally promoted by aluminum-based Lewis acid sites (LAS).[13,15] However, the observation of formaldehyde along with carbon monoxide (CO) and hydrogen (H_2) upon passing methanol feed over BAS-free materials, such as silicalite, Na-ZSM-5,

Received: June 19, 2022
Revised: August 23, 2022
Published: October 19, 2022

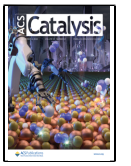

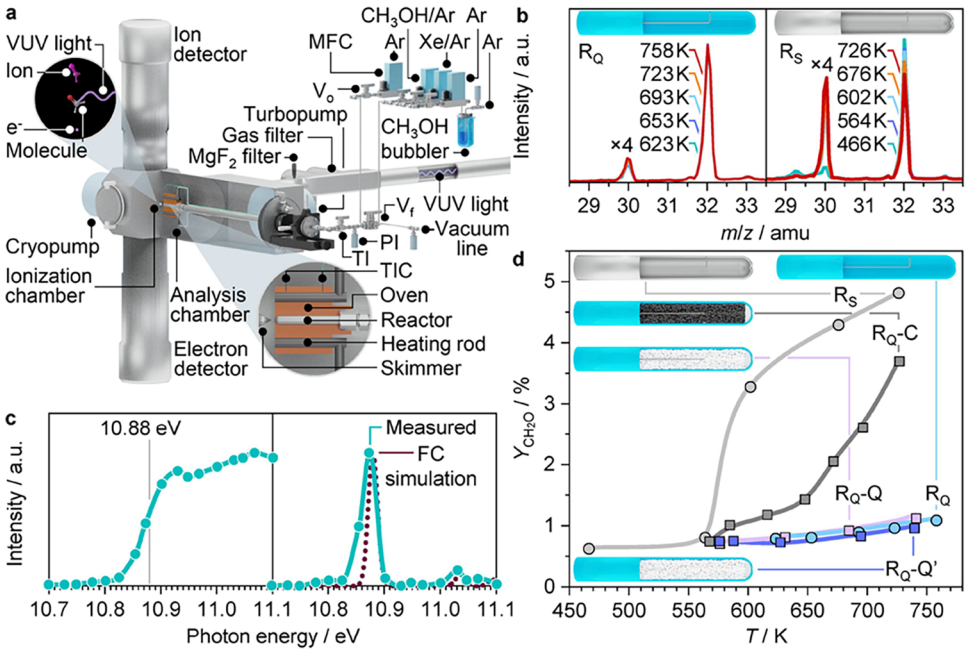

Figure 1. (a) Schematic of the reactor setup coupled with i^2PEPICO spectroscopy. V_o: one-way valve, V_f: four-way valve, PI: pressure indicator, TI: temperature indicator, TIC: temperature indicator controller, and MFC: mass flow controller. (b) Time-of-flight (TOF) spectra in the m/z 29−33 range, recorded in empty quartz (R_Q, left) and stainless steel (R_S, right) reactors at different temperatures at photon energy of $h\nu$ = 10.9 eV. The m/z 30 signal is multiplied four times for clarity. (c) Photoionization (left) and mass-selected threshold photoelectron spectra (ms-TPES, right) of m/z 30 species recorded in a stainless steel reactor at 676 K. Frank−Codon simulation of ms-TPES of formaldehyde is shown for comparison. (d) Formaldehyde yield versus temperature in the methanol reaction in empty quartz (R_Q) and stainless steel (R_S) reactors, quartz reactors loaded with silicon carbide (R_Q-C) or quartz particles (R_Q-Q), and a quartz reactor filled with quartz without a thermocouple (R_Q-Q′). Reaction conditions: $W_{Q,C}$ = 0.100 g, CH_3OH:Xe:Ar = 2.3:0.15:97.55 mol %, F_T = 20 cm^3_{STP} min^{-1}, P = 0.5 bar, and T = 466−758 K.

quartz, and silicon carbide, indicated that alternative pathways can also contribute to aldehyde production.[19,25] It was thereby speculated that structural defects in these materials can catalyze methanol disproportion or dehydrogenation.[19] The seldom quantification of the formaldehyde productivity over the BAS-free materials indicated that it is ca. 2−10 times lower in comparison to MTH catalysts.[19,25] Alternatively, formaldehyde may also arise from methanol dehydrogenation catalyzed by transition metals.[27−32] In this regard, it is worth noting that industrial reactors and accompanying equipment are commonly made of stainless steel,[33,34] which may exhibit dehydrogenation activity. Indeed, some patents report that covering the stainless steel walls with protective layers can improve the lifetime of the MTH catalysts.[34] However, despite its fundamental and practical relevance, the wall-catalyzed formaldehyde formation and its role in the MTH reaction have not yet been systematically investigated. This is largely caused by the challenging detection of formaldehyde in the MTH conversion, because of its low concentration and facile decomposition in gas chromatography and electron ionization mass spectrometry.[35,36] Similarly, interferences and tedious sample preparation complicate the formaldehyde analysis by alternative quantification methods, such as infrared and UV−vis analysis.[19,21,37]

Herein, we exploited the double-imaging photoelectron photoion coincidence spectroscopy (i^2PEPICO) to systematically analyze the production of formaldehyde in empty quartz and stainless steel reactors as well as over representative bed diluents and zeolite catalysts. In comparison to other techniques, photoionization techniques, such as i^2PEPICO, allow for fragmentation-free soft ionization at high sampling frequency.[25,38−41] Combined with molecular beam sampling, which reduces the number of molecular collisions and suppresses chemical reactions after the sample leaves the reactor, i^2PEPICO enables highly sensitive formaldehyde detection in the gas phase also in the presence of MTH products and intermediates. The results show that transition-metal sites in stainless steel walls and silicon carbide diluents catalyze the methanol dehydrogenation to formaldehyde, wherein the formaldehyde yields can exceed those of the zeolite-catalyzed HT pathways. The formaldehyde obtained by the wall-catalyzed reactions promotes the arene HP and PAHs formation over MTH catalysts, eventually reducing catalyst lifetime and the propene-to-ethene product ratio.

2. EXPERIMENTAL SECTION

2.1. Materials and Characterization. Silicon carbide (Alfa Aesar, 0.250−0.325 mm) and quartz (Thommen-Furler, 0.250−0.325 mm), denoted as C and Q, respectively, were calcined under static air at 873 K. Stainless steel chips (0.25−1.8 mm), denoted as S, were obtained by machining of a stainless steel tube (Swagelok) and then thermally treated under nitrogen flow at 773 K. ZSM-5 catalysts with nominal Si/Al ratios of 15 (Zeolyst, CBV 3024E) and 40 (Zeolyst, CBV 8014) and the Beta catalyst with a nominal Si/Al ratio of 19 (Zeolyst, CP814C), denoted as Z_{15}, Z_{40}, and B_{19}, respectively, were transformed from ammonium to protonic form by calcination under oxygen flow at 823 K. Calcium-modified ZSM-5 with a nominal loading of 2 wt %, denoted as CaZ_{40}, was prepared by dry impregnation of the Z_{40} material using an aqueous solution of $Ca(NO_3)_2 \times 4H_2O$ (Sigma-Aldrich, >99%), followed by drying at 30 mbar and 353 K for 12 h and calcination at 823 K. All calcinations and thermal treatments were performed for 5 h using a heating rate of 2

https://doi.org/10.1021/acscatal.2c02953
ACS Catal. 2022, 12, 13426−13434

K min^{-1}. The materials were characterized by powder X-ray diffraction (PXRD), scanning electron microscopy with energy dispersive X-ray (SEM−EDX) analysis, X-ray photoemission spectroscopy, and Fourier transform infrared (FTIR) spectroscopy, which are detailed in the Supporting Information.

2.2. *i*²PEPICO Spectroscopy Experiments. *i*²PEPICO spectroscopy experiments were performed at the vacuum ultraviolet (VUV) beamline of the Swiss Light Source (Figure 1a).[38,42−44] Argon (Ar, PanGas, 5.0 used as the diluent) and xenon (Xe, 2% in Ar, Messer, 5.0, used as the internal calibrant) were fed by digital mass flow controllers (Bronkhorst). Diluted methanol vapor was introduced by passing the argon flow through a methanol bubbler, placed in a water thermostat maintained at a constant temperature of 280 K. The inlet feed was supplied to a four-way valve, from where it was either directed to an exhaust vacuum line for stabilization, or to the stainless steel or quartz reactors with an outlet pinhole for the catalytic measurements. In the case of the stainless steel reactor, an auxiliary stainless steel tube, concentrically positioned in the interior, was used to introduce the catalyst. The catalyst was deposited on the inner and outer surface of the tube by wash-coating with zeolite suspension in ultrapure water (Milli-Q), followed by drying under vacuum (30 mbar) at 353 K for 12 h. In the case of a quartz reactor, silicon carbide, quartz, or a mixture of zeolite and quartz particles were loaded in the form of fixed bed. A thin layer of quartz wool was placed at the outlet of both reactors to preclude the potential loss of the loaded solids. The reactor temperature was set by a home-made resistively heated electric oven, which was connected to two Type K thermocouples and a PID controller. The reactor temperature was monitored by a Type K thermocouple, the tip of which was positioned in the center of the catalyst-free reactor, auxiliary tube, or packed bed. The reaction pressure was monitored by a pressure transducer above the reaction zone. Prior to the experiment, the reactors were thermally treated under an argon flow at 773 K for 0.5 h to remove any potentially present organic impurities. Unless otherwise stated, the *i*²PEPICO spectroscopy experiments were performed in the temperature range of T = 466−758 K at P = 0.5 bar by feeding F_T = 20 cm^3_{STP} min^{-1} of the reaction mixture of the composition CH_3OH:Xe:Ar = 2.3:0.15:97.55 mol %, which, in the case of zeolite catalysts, resulted in a weight-hourly space velocity (*WHSV*) of 3.8 or 6.4 g_{CH3OH} g_{cat}^{-1} h^{-1}.

The molecular beam leaving the reactor was skimmed and fed in the analysis chamber operated at 2×10^{-9} bar, wherein it was ionized by VUV synchrotron radiation. The radiation was dispersed by a 150 mm^{-1} grating working in grazing incidence to monochromatize the light. The second-order radiation was suppressed in the 9−14 eV range by an Ar in Ne mixture (Carbagas, 25 mol % Ar in Ne 5.0) in the gas filter operating at 1×10^{-2} bar over an optical length of 10 cm. For the analysis performed at 10.6 eV, higher-order radiation was quantitatively suppressed by a MgF_2 filter. The photoions and photoelectrons from the photoionization are accelerated vertically in opposite directions by a constant electric field of 213 V cm^{-1} toward two delay-line anode detectors (Roentdek, DLD40). They were velocity map imaged and detected in delayed coincidence. Further details of the methanol and product analysis are provided in the Supporting Information.

2.3. Methanol Conversion Experiments. Methanol conversion over stainless steel chips was analyzed in a fixed-bed reactor by using CH_3OH:He = 3.7:96.3 mol %, *WHSV* = 0.8 g_{CH3OH} g_s^{-1} h^{-1}, T = 673−823 K, and P = 1.0 bar. MTH conversion was performed by using CH_3OH:Ar = 5.6:94.4 mol %, *WHSV* = 119 g_{CH3OH} g_{Z15}^{-1} h^{-1} or 95 g_{CH3OH} g_{Z40}^{-1} h^{-1} at T = 673 K (Z_{15}) or 723 K (Z_{40}) and P = 1.6 bar. Further details of the reactor setups, catalytic tests, and analysis protocols are provided in the Supporting Information.

3. RESULTS AND DISCUSSION

3.1. Nonzeolite-Catalyzed Formation of Formaldehyde. The analysis of the formaldehyde formation was commenced by assessing the methanol conversion in empty stainless steel (R_S) and quartz (R_Q) reactors, because these are typically used to construct laboratory and industrial units for MTH conversion, respectively.[13,19,21,33] The experiments were performed by placing the reactors inside the source chamber of the *i*²PEPICO endstation (Figure 1a). The reaction of methanol was analyzed in the temperature range of ca. 466−758 K at a total pressure of ca. 0.5 bar, which are comparable conditions to those applied in the laboratory testing of the MTH catalysts.[13,21,23] By choosing the photoionization energy of $h\nu$ = 10.9 eV, the fragmentation of formaldehyde could be suppressed, thus allowing for its selective detection in the presence of methanol and the MTH products.[25,36] In particular, the time-of-flight (TOF) mass spectra of the outlet reactor feed recorded at $h\nu$ = 10.9 eV revealed that, besides the characteristic methanol peak at m/z 32 and its small ^{13}C satellite at m/z 33, an additional peak was also present at m/z 30 (Figure 1b). Because this photoionization energy is well below the dissociative ionization threshold of methanol, the m/z 30 peak arises from formaldehyde.[25,36] This is also verified by the photoionization and mass-selected threshold photoionization spectra (ms-TPES) of the m/z 30 signal, which match those of formaldehyde (Figure 1c).[25,36,45] Comparatively, the intensity of the peak at m/z 30 recorded through a quartz reactor at room temperature was at the level of the background noise. At increased reaction temperatures, the formaldehyde yield reached 0.9 mol % in the quartz reactor. In contrast, the formaldehyde yield increased to ca. 4.8 mol % in the stainless steel reactor, with a very prominent rise at ca. 600 K. This unequivocally evidences that stainless steel walls catalyze methanol transformation into formaldehyde. Because of this intriguing outcome, the formaldehyde evolution was also investigated over quartz and coarse silicon carbide particles packed inside the quartz reactor, as these are commonly used bed diluents in laboratory testing of the MTH catalysts (Figures 1d and S1).[6,13,23] The production of formaldehyde over the bed of a quartz particles was similar to that of an empty quartz reactor and was not affected by the presence of the thermocouple, thus ruling out the substantial contribution of the latter on this reaction. In contrast, the activity of coarse silicon carbide was significantly higher, attaining the yields of ca. 2.0−3.6% in the temperature range of 675−730 K.

3.2. Mechanism of the Nonzeolite-Catalyzed Formation of Formaldehyde. To assess the origin of the high formaldehyde yield over stainless steel and coarse silicon carbide with respect to quartz, the bulk compositions of these materials were assessed by energy-dispersive X-ray (EDX) spectroscopy (Figure S2). As expected, iron was identified as the main component of steel, while the other major components were present in a molar ratio of ca. Fe:Cr:Ni:Mn:Si:C = 1:0.29:0.18:0.02:0.03:0.31. The analysis also revealed that the coarse silicon carbide contained small amounts of iron, with an estimated molar composition of

https://doi.org/10.1021/acscatal.2c02953
ACS Catal. 2022, 12, 13426−13434

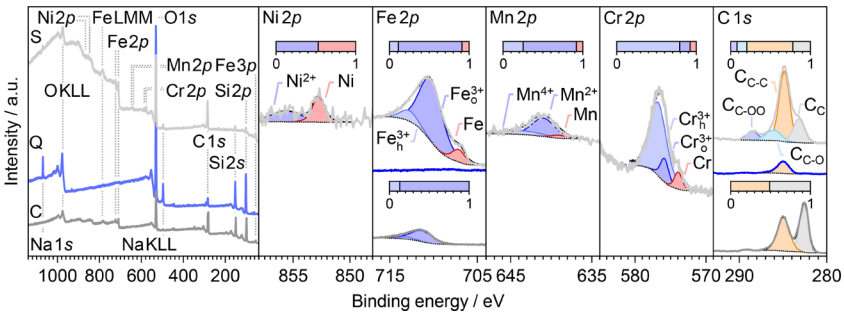

Figure 2. Survey and selected Ni 2*p*, Fe 2*p*, Mn 2*p*, Cr 2*p*, and C 1*s* core-level X-ray photoemission spectra of stainless steel chips (S), crude silicon carbide (C), and quartz (Q) particles. Insets indicate the fractions of respective peak components. Indexes o and h in designations of peak components indicate oxide and hydroxide, respectively.

Si:C:Fe = 1:0.84:0.07. Inactive quartz particles showed no traceable metal impurities, except for sodium. X-ray photoelectron spectroscopy (XPS, Figure 2, Table S1) corroborates these results. In particular, iron and chromium are the most abundant metal components in the surface layers of a stainless steel, while manganese and nickel were present in substantially smaller quantities. Herein, Fe 2*p*, Cr 2*p*, and Mn 2*p* core-level spectra indicate that these metals are mainly present in the oxide form, although the iron and chromium signals also display low-intensity contributions arising from the corresponding metal components. The Ni 2*p* core-level spectra suggest that this element is mostly in metallic form on the surface. The XPS data imply the presence of a passive iron-chromium surface oxide film, which is the characteristic surface composition of the stainless steel materials.[46] Therein, a ca. 1.7 nm thick iron oxide-rich layer is present at the surface and is followed by ca. 1.8 nm thick subsurface layer of chromium oxide layer. The photoelectron spectra of the silicon carbide material also revealed the presence of iron in both metallic and oxide forms, whereas the spectra of quartz excluded the presence of transition metals.

The bulk and surface compositional analysis indicated a positive correlation between formaldehyde production and the presence of transition metal centers (Figure 1d), which implies a high activity of the latter sites, especially in view of the low surface area and small iron content of silicon carbide. This observation is also consistent with the reported activity of several noble and transition metal catalysts in methanol dehydrogenation.[27−32] Density functional theory (DFT) analysis of the methanol decomposition over metal surfaces indicates that methanol can be activated via scission of the C−O, C−H, or O−H bonds, in the order of decreasing activation energy.[27−29,31] The dissociation of the O−H bond leads to the formation of surface hydrogen (H*) and methoxy (CH_3O*) species.[30,31] Hydride transfer from the latter yields surface-bound formaldehyde, which may further decompose into carbon monoxide and hydrogen. DFT calculations also indicated that formaldehyde exhibits the lowest adsorption energy of all the surface-bound intermediates, which opens up the possibility for its facile desorption.[30,31]

To gain insights into the mechanism of formaldehyde formation over the stainless steel reactor walls, the byproducts were also analyzed (Figure 3a). Methane was detected at photon energy of $h\nu$ = 13.9 eV. However, its yield was ca. 2−10 times lower than that of formaldehyde, with a marginal increase over the investigated temperature range. These results implicate a small contribution of the methanol disproportionation reaction. On the other hand, the yield of CO was ca. 4−

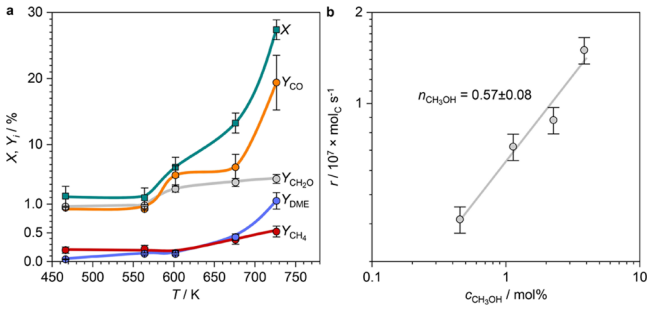

Figure 3. (a) Conversion (X) and product yields (Y_i) versus temperature, and (b) apparent reaction order at T = 676 K in the methanol reaction in empty stainless steel (R_S) reactor. Methanol concentration in (b) was varied in the range of CH_3OH:Xe:Ar = 0.5-3.9:0.15:99.35−95.95 mol %. Other conditions correspond to those reported in the caption of Figure 1.

6 times higher than that of formaldehyde. Consistent with this, hydrogen can be unequivocally detected in the methanol reaction over the stainless steel chips performed in the laboratory reactor setup (Figure S3). These results corroborate the assumption that formaldehyde is generated as an intermediate product in the methanol dehydrogenation into carbon monoxide. Higher CO production compared with methane resembles the typical product distribution observed in the methanol dehydrogenation over the transition metal catalysts.[29,31] In addition, it is also consistent with the findings of the DFT analysis indicating that the scission of the O−H and C−H bonds is favored over the dissociation of the C−O bond.[27−29] The rate of methanol consumption in the stainless steel reactor displays an apparent reaction order of ca. 0.5 with respect to the partial pressure of this reactant. This kinetic behavior can be explained by the simplified reaction mechanism in which the dissociation of C−H bonds following O−H bond scission is likely the rate-limiting step (see Supporting Discussion 2.1 for details).[31]

3.3. Impact of Nonzeolite-Catalyzed Formaldehyde Formation on the MTH Reaction. We have evidenced a substantial activity of stainless steel walls in methanol dehydrogenation. What is the impact of the wall-catalyzed formaldehyde formation on the overall MTH reaction? This question was first approached by comparing formaldehyde yields via wall- and zeolite-catalyzed reactions. The production of formaldehyde was studied over the ZSM-5 catalyst with a Si:Al ratio of 40 under the conditions used to investigate the activity of the reactor walls and diluents. Two reactor configurations were considered (Figure 4). In the first

https://doi.org/10.1021/acscatal.2c02953
ACS Catal. 2022, 12, 13426−13434

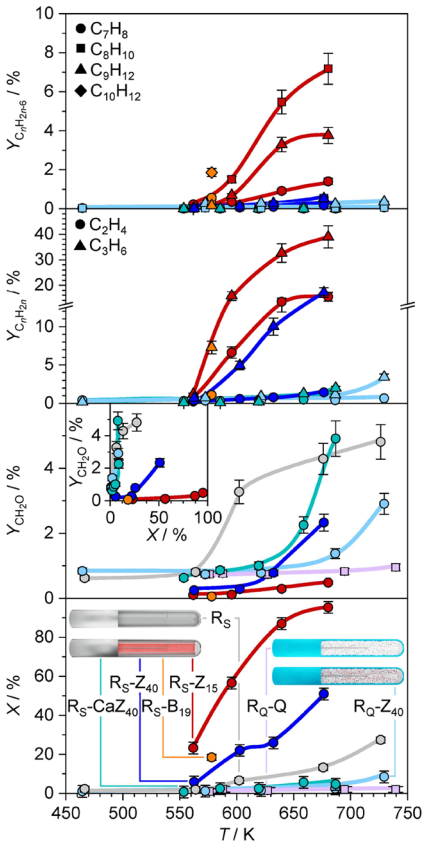

Figure 4. Conversion and yields of formaldehyde, alkenes, and methylated benzenes versus temperature in MTH conversion over Z_{15}, Z_{40}, CaZ_{40}, and B_{19} catalysts in a stainless steel reactor and Z_{40} catalyst in a quartz reactor. The activity profiles of the empty stainless steel reactor (R_S) and quartz reactor loaded with quartz (R_Q-Q) are included for comparison. The inset presents the formaldehyde yield versus conversion which was varied by changing the reaction temperature. Conditions: *WHSV* = 6.4 (R_Q-Z_{40}) or 3.8 g_{CH3OH} g_{cat}^{-1} h^{-1} (other catalysts), CH_3OH:Xe:Ar = 2.3:0.15:97.55 mol %, *P* = 0.5 bar, and *T* = 466−730 K.

arrangement (R_Q-Z_{40}), the catalyst was well-mixed with quartz particles displaying low formaldehyde formation activity. The amount of the ZSM-5 catalyst was adjusted to operate the reaction at incomplete methanol conversion (≤5%), which minimizes the consumption of formaldehyde through secondary reactions with MTH products. The formaldehyde yield in this reactor was higher than over the bed of quartz particles in the temperature range above ca. 650 K, indicating the activity of the zeolite acid sites in the formation of this intermediate. However, the yield of formaldehyde over the Z_{40} catalyst was smaller than in the empty stainless steel reactor. Notably, the light-off curve in the case of the Z_{40} catalyst is shifted to ca. 130 K higher temperature in comparison to the empty stainless steel reactor and to ca. 50 K higher temperature in comparison to silicon carbide. This indicates that under similar reaction conditions, the reactivity of the stainless steel and silicon carbide is at least comparable to, but likely higher than the reactivity of the acid sites of zeolites, which is also corroborated by estimating the activities of acid and metal sites (please see Supporting Discussion 2.2). In the second reactor configuration, a stainless steel tube was wash-coated with a catalyst and loaded inside the stainless steel reactor (R_S-Z_{40}). Here, the formaldehyde yield was also lower than in the empty stainless steel-reactor. However, in this case, the conversion of methanol and the yields of MTH products were significantly higher in comparison to the fixed-bed reactor configuration.

To assess how the stainless steel walls and zeolite catalysts interact and influence formaldehyde formation and reactivity, the formaldehyde production was also evaluated over several zeolites at constant *WHSV* using the wash-coated reactor configuration (Figure 4). The activities of the catalysts increased in the order CaZ_{40} < Z_{40} < B_{19} < Z_{15}, correlating with increasing acid site concentration and differences in inherent framework activities of ZSM-5 and BEA zeolites (Table S2, Figures S4 and S5). Formaldehyde yields over highly active Z_{15} and B_{19} zeolites (0.1−0.5 mol %) were significantly lower in comparison to the Z_{40} catalyst and empty reactor, also in the low conversion regime. On the other side, the formaldehyde yields over CaZ_{40} exhibited very low MTH activity due to high fraction of poisoned BAS with regard to the parent Z_{40} material. Herein, the formaldehyde yields approached those in an empty stainless steel reactor in the high-temperature range. These results imply a negative correlation between the apparent formaldehyde yield and the MTH activity, which is also observable from the formaldehyde yield versus conversion profiles (Figure 4, inset). A significantly lower yield of formaldehyde over zeolite catalysts loaded in a stainless steel reactor in comparison to the empty stainless steel reactor can be caused by the competitive MTH conversion over zeolite, which reduces the amount of methanol available for dehydrogenation on the reactor walls. In addition, it can also arise from the fast consumption of formaldehyde generated by the reactor walls via the MTH reaction network. In principle, both pathways are likely to exist in parallel. Notably, the yields of formaldehyde over zeolite catalysts in the stainless steel reactor at methanol conversions of ca. 18−25% are 8−12 times lower than in an empty stainless steel reactor under similar temperature conditions (Figure 4). Such a difference in formaldehyde productivity is more pronounced than the maximum estimated to arise from a decrease of methanol concentration because of the parallel MTH reaction (≤2.6 times, please see Supporting Discussion 2.3). This implies that formaldehyde is consumed through reactions with hydrocarbon products, which is consistent with catalytic tests involving stainless steel chips and formaldehyde cofeeding (vide infra) and previous reports on the high reactivity of this intermediate.[22,26] In addition, the analysis also suggests that in the stainless steel reactor loaded with a zeolite catalyst the consumption of formaldehyde has at least a comparable impact on the decrease of its yield as the competitive MTH conversion (please see Supporting Discussion 2.3). Consistent with previous reports, the *i*^{2}PEPICO analysis also shows that Z_{15} and B_{19} catalysts exhibit a high propensity toward ethylene and aromatics, which arise from the reactions of the arene HP carriers. Low formaldehyde yield over Z_{15} and B_{19} can thus be associated with an increased concentration of the aromatic-chain carriers, their precursors, and plausibly their high propensity to react with this methanol derivative.

At this point, it is interesting to note that the onset of the hydrocarbon formation displays a shift toward lower (>100 K) temperature in the wash-coated stainless steel reactor in comparison to the quartz reactor loaded with the Z_{40} catalyst, although *WHSV* is only ca. 1.7 times smaller in the former case. Consistent with this, the addition of formaldehyde to the

https://doi.org/10.1021/acscatal.2c02953
ACS Catal. 2022, 12, 13426−13434

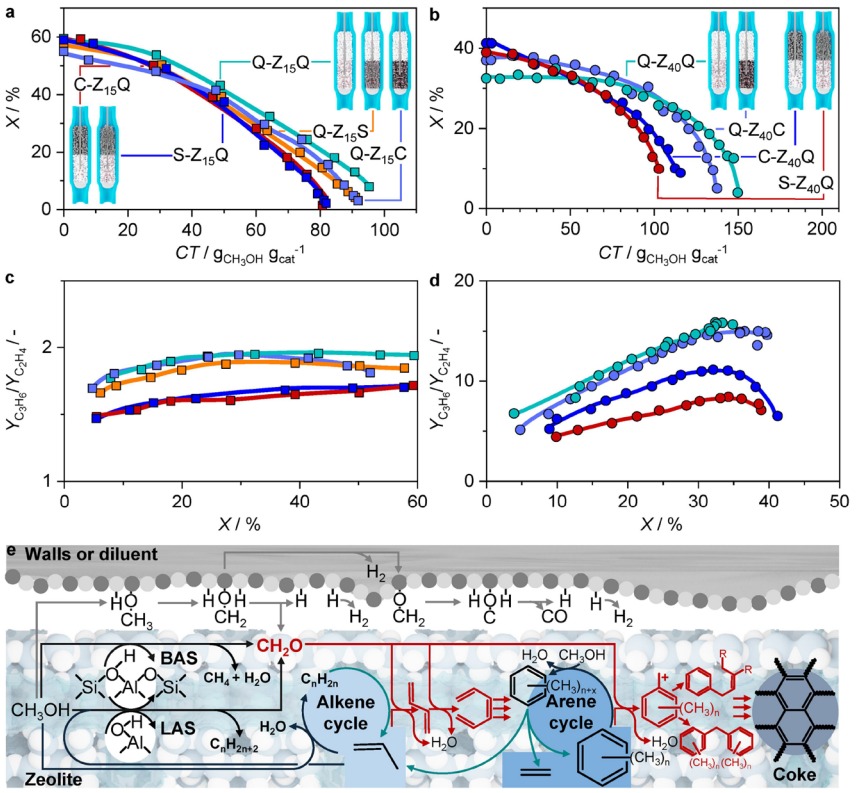

Figure 5. (a,b) Conversion versus cumulative turnover (*CT*) capacity and (c,d) ratio of the propylene and ethylene yields (Y_{C3H6}/Y_{C2H4}) in the MTH reaction over (a,c) Z_{15} and (b,d) Z_{40} catalysts in different reactor configurations: mixed catalyst-quartz bed below the prebeds of quartz (Q-Z_{15}Q, Q-Z_{40}Q), stainless steel (S-Z_{15}Q, S-Z_{40}Q), or silicon carbide (C-Z_{15}Q, C-Z_{40}Q), and quartz prebed on top of mixed catalyst-stainless steel (Q-Z_{15}S, Q-Z_{40}S) or catalyst-silicon carbide beds (Q-Z_{15}C). Conditions: *WHSV* = 119 g_{CH3OH} g_{Z15}^{-1} h^{-1} or 95 g_{CH3OH} g_{Z40}^{-1} h^{-1}, CH_3OH:Ar = 5.6:94.4 mol %, *P* = 1.6 bar, and *T* = 673 K (Z_{15}) or 723 K (Z_{40}). (e) Mechanistic scheme summarizing the formation of formaldehyde and its involvement in the dual-cycle HP mechanism of the MTH transformation.

methanol feed led to a significant reduction of the induction period in the MTH reaction over Z_{40} zeolite (Figure S6). These observations suggest that the formaldehyde generated by the nonzeolite-catalyzed reaction may promote the formation of the hydrocarbon pool, which is in agreement with the recent reports revealing the important role of this methanol derivative in the synthesis of the first C−C bond.[16,17,19,21]

The *i*²PEPICO results indicate that the production of formaldehyde over stainless steel and silicon carbide can be substantial and that produced formaldehyde is consumed by the MTH reaction. Further corroboration of these findings was obtained by evaluating the performance of the representative Z_{15} and Z_{40} catalysts in the presence of stainless steel chips, coarse silicon carbide, and quartz particles using different fixed-bed reactor configurations (Figure 5). Mixing of Z_{15} zeolite particles with carbide and stainless steel chips led to a slightly (ca. 10%) reduced *CT* capacity in comparison to a mixed quartz-zeolite bed (Figure 5a). Comparatively, the addition of these materials in the form of prebeds led to a more prominent drop of the *CT* capacity (ca. 20%) of the same catalyst. Similarly, the prebeds containing stainless steel chips and coarse silicon carbide particles caused a prominent decrease of the *CT* capacity of the Z_{40} catalyst, while the mixed coarse silicon carbide-Z_{40} bed led to a small decrease of the catalyst lifetime (Figure 5b). In addition to affecting the *CT* values, the stainless steel and silicon carbide prebeds are also inducing changes in the product distribution, which are especially reflected by the decreased propene over ethene yield (Figure 5c,d). Similar to the effects of stainless-steel chips and silicon carbide particles, cofeeding formaldehyde with methanol over a mixed quartz-Z_{40} bed caused a decrease of the *CT* capacity as well as propene over ethene yield (Figure S7). Contrastingly, no significant changes in activity and selectivity profile were observed when carbon monoxide and hydrogen were added to the methanol feed over the same catalyst under identical conditions (Figure S7). These control experiments imply that the impact of stainless steel chips and silicon carbide particles on the MTH transformation is primarily associated with the formation of formaldehyde over these materials. This is well-aligned with previous studies indicating that hydrogen and mixed hydrogen-carbon monoxide cofeeds can enhance the catalyst lifetime in the MTH reaction only at high partial pressures (ca. 5−19 bar).[24,47] In contrast, small quantities of formaldehyde led to a prominent decrease of the MTH turnover capacity and selectivity to C_{3+} alkenes.[7,21] Formaldehyde fosters the transformation of alkene-chain carriers into dienes and polyenes via Prins or hydroacylation reactions. These unsaturated hydrocarbons are then readily transformed to aromatics (Figure 5e).[13,21,22] As a result, methanol dehydrogenation into formaldehyde increases the relative concentration of arene with respect to alkene-mediated reactions. Because ethylene is produced via the reactions of arene HP, whereas propene is obtained through both alkene and arene HPs,[1,3] the observation of the decreased propylene-to-ethylene ratio in the presence of stainless steel chips and crude silicon carbide implicates the increased arene- over the alkene-based chain carriers. This, along with the promoting

https://doi.org/10.1021/acscatal.2c02953
ACS Catal. 2022, 12, 13426−13434

effect of formaldehyde on the condensation of monocyclic into inactive polycyclic hydrocarbons, that is, coke, also rationalizes the increased deactivation.[13,21−23] A more pronounced decrease of the turnover capacity and propene to ethene ratio in the case of prebed with respect to mixed-bed configurations involving stainless steel chips and silicon carbide particles can be rationalized by the competition between the methanol dehydrogenation and MTH conversion. Namely, in the case of a prebed, the entire methanol feed is only reacting via the dehydrogenation pathway, which maximizes the productivity of formaldehyde. In the case of mixed-beds, significant part of methanol is consumed in the MTH transformation, which reduces its average concentration, and hence decreases the yield of formaldehyde (Figure 3b).

4. CONCLUSIONS

In this work, we demonstrated that stainless steel walls and coarse silicon carbide particles catalyze the methanol-to-formaldehyde conversion, attaining productivities higher than or comparable to those of the HT reactions catalyzed by the zeolite acid sites under comparable reaction conditions (Figure 5e). The formaldehyde formation over the former two materials proceeds via the dehydrogenation pathway catalyzed by transition metals and is accompanied by the production hydrogen and carbon monoxide as byproducts (Figure 5e). The comparatively high activity of steel and silicon carbide with respect to quartz implies the essential role of transition metals in catalyzing methanol dehydrogenation. The formaldehyde produced via this reaction fosters the formation of dienes, polyenes, and aromatics, thus enhancing the arene HP and catalyst deactivation (Figure 5e). A comparatively low yield of formaldehyde over the zeolites with high BAS concentration indicates its high reactivity with these catalysts, which can be ascribed to the higher concentration of the arene intermediates. These results demonstrate that besides the catalyst and applied reaction conditions, bed diluents and the walls of reactors and various upstream equipment that comes in contact with the heated methanol feed can impact the catalyst stability and product distribution through the formaldehyde-mediated reactions. The magnitude of the non-zeolite-catalyzed reactions is dependent on the reactor surface and on the type of diluent. Our experiments showed that the quartz reactor and diluents free of metal impurities minimize the nonzeolite-catalyzed evolution of formaldehyde and should be therefore used to investigate the formation of formaldehyde over zeolite catalysts. Still, the background activity of the zeolite-free reactor should be always assessed. In addition, the formation of formaldehyde should be performed in the low-conversion regime, wherein the outlet concentration of this intermediate is not affected by its conversion through the reactions with MTH products. The findings are also relevant for the industrial application of the MTH technology, because stainless steel is used as a ubiquitous construction material. With this in mind, the application of protective layers should be considered as a strategy to enhance the MTH performance.

■ ASSOCIATED CONTENT

Supporting Information

The Supporting Information is available free of charge at https://pubs.acs.org/doi/10.1021/acscatal.2c02953.

Additional experimental details, supplementary discussion of the mechanism of methanol-to-formaldehyde dehydrogenation, surface composition of stainless steel chips, crude silicon carbide, and quartz particles, textural and acid properties of zeolite catalysts, PXRD, SEM−EDX, FTIR analyses, methanol conversion experiments over stainless-steel chips, and additional MTH experiments (PDF)

■ AUTHOR INFORMATION

Corresponding Author

Vladimir Paunović − *Institute for Chemical and Bioengineering, ETH Zurich, 8093 Zurich, Switzerland; Laboratory for Catalysis and Sustainable Chemistry, Paul Scherrer Institute, 5232 Villigen, Switzerland;* orcid.org/0000-0001-6630-1672; Email: vladimir.paunovic@chem.ethz.ch

Authors

Patrick Hemberger − *Laboratory for Synchrotron Radiation and Femtochemistry, Paul Scherrer Institute, 5232 Villigen, Switzerland;* orcid.org/0000-0002-1251-4549

Andras Bodi − *Laboratory for Synchrotron Radiation and Femtochemistry, Paul Scherrer Institute, 5232 Villigen, Switzerland;* orcid.org/0000-0003-2742-1051

Roland Hauert − *Swiss Federal Laboratories for Materials Science and Technology, EMPA, 8600 Dübendorf, Switzerland*

Jeroen A. van Bokhoven − *Institute for Chemical and Bioengineering, ETH Zurich, 8093 Zurich, Switzerland; Laboratory for Catalysis and Sustainable Chemistry, Paul Scherrer Institute, 5232 Villigen, Switzerland;* orcid.org/0000-0002-4166-2284

Complete contact information is available at: https://pubs.acs.org/10.1021/acscatal.2c02953

Author Contributions

V.P. conceived the idea, performed the i^2PEPICO experiments and MTH catalytic tests, analyzed the data, and coordinated this project. P.H. and A.B. supported the planning and execution of the i^2PEPICO experiments and discussed the i^2PEPICO data. R.H. conducted the XPS analysis. J.A.v.B. discussed the data. V.P. wrote the manuscript with comments and corrections from all the authors.

Notes

The authors declare no competing financial interest.

■ ACKNOWLEDGMENTS

We acknowledge the VUV beamline of the Swiss Light Source at Paul Scherrer Institute (PSI), Villigen, Switzerland for granting a beamtime, Mr. Zeyou Pan and Mr. Patrick Ascher from PSI for technical assistance during the i^2PEPICO measurements, Mr. Charles Pare and Dr. Przemyslaw Rzepka from ETH Zurch for help with MS and SEM−EDX analysis, ScopeM at ETH Zurich for the access to the SEM facility, and the Energy System Integration platform of the PSI for financial support.

■ REFERENCES

(1) Olsbye, U.; Svelle, S.; Bjrgen, M.; Beato, P.; Janssens, T. V. W.; Joensen, F.; Bordiga, S.; Lillerud, K. P. Conversion of Methanol to Hydrocarbons: How Zeolite Cavity and Pore Size Controls Product Selectivity. *Angew. Chem., Int. Ed.* **2012**, *51*, 5810−5831.

(2) Tian, P.; Wei, Y.; Ye, M.; Liu, Z. Methanol to Olefins (MTO): From Fundamentals to Commercialization. *ACS Catal.* **2015**, *5*, 1922−1938.
(3) Yarulina, I.; Chowdhury, A. D.; Meirer, F.; Weckhuysen, B. M.; Gascon, J. Recent Trends and Fundamental Insights in the Methanol-to-Hydrocarbons Process. *Nat. Catal.* **2018**, *1*, 398−411.
(4) Ilias, S.; Bhan, A. Mechanism of the Catalytic Conversion of Methanol to Hydrocarbons. *ACS Catal.* **2013**, *3*, 18−31.
(5) Van Speybroeck, V.; De Wispelaere, K.; Van Der Mynsbrugge, J.; Vandichel, M.; Hemelsoet, K.; Waroquier, M. First Principle Chemical Kinetics in Zeolites: The Methanol-to-Olefin Process as a Case Study. *Chem. Soc. Rev.* **2014**, *43*, 7326−7357.
(6) Müller, S.; Liu, Y.; Vishnuvarthan, M.; Sun, X.; Van Veen, A. C.; Haller, G. L.; Sanchez-Sanchez, M.; Lercher, J. A. Coke Formation and Deactivation Pathways on H-ZSM-5 in the Conversion of Methanol to Olefins. *J. Catal.* **2015**, *325*, 48−59.
(7) Martinez-Espin, J. S.; Mortén, M.; Janssens, T. V. W.; Svelle, S.; Beato, P.; Olsbye, U. New Insights into Catalyst Deactivation and Product Distribution of Zeolites in the Methanol-to-Hydrocarbons (MTH) Reaction with Methanol and Dimethyl Ether Feeds. *Catal. Sci. Technol.* **2017**, *7*, 2700−2716.
(8) Lee, S.; Choi, M. Unveiling Coke Formation Mechanism in MFI Zeolites during Methanol-to-Hydrocarbons Conversion. *J. Catal.* **2019**, *375*, 183−192.
(9) Valecillos, J.; Vicente, H.; Gayubo, A. G.; Aguayo, A. T.; Castaño, P. Spectro-Kinetics of the Methanol to Hydrocarbons Reaction Combining Online Product Analysis with UV-Vis and FTIR Spectroscopies throughout the Space Time Evolution. *J. Catal.* **2022**, *408*, 115−127.
(10) Wei, Y.; Yuan, C.; Li, J.; Xu, S.; Zhou, Y.; Chen, J.; Wang, Q.; Xu, L.; Qi, Y.; Zhang, Q.; Liu, Z. Coke Formation and Carbon Atom Economy of Methanol-to-Olefins Reaction. *ChemSusChem* **2012**, *5*, 906−912.
(11) Barbera, K.; Sorensen, S.; Bordiga, S.; Skibsted, J.; Fordsmand, H.; Beato, P.; Janssens, T. V. W. Role of Internal Coke for Deactivation of ZSM-5 Catalysts after Low Temperature Removal of Coke with NO_2. *Catal. Sci. Technol.* **2012**, *2*, 1196−1206.
(12) Paunović, V.; Sushkevich, V.; Rzepka, P.; Artiglia, L.; Hauert, R.; Sik Lee, S.; van Bokhoven, J. A. Reactivation of Catalysts for Methanol-to-Hydrocarbons Conversion with Hydrogen. *J. Catal.* **2022**, *407*, 54−64.
(13) Müller, S.; Liu, Y.; Kirchberger, F. M.; Tonigold, M.; Sanchez-Sanchez, M.; Lercher, J. A. Hydrogen Transfer Pathways during Zeolite Catalyzed Methanol Conversion to Hydrocarbons. *J. Am. Chem. Soc.* **2016**, *138*, 15994−16003.
(14) Martínez-Espín, J. S.; De Wispelaere, K.; Janssens, T. V. W.; Svelle, S.; Lillerud, K. P.; Beato, P.; Van Speybroeck, V.; Olsbye, U. Hydrogen Transfer versus Methylation: On the Genesis of Aromatics Formation in the Methanol-To-Hydrocarbons Reaction over H-ZSM-5. *ACS Catal.* **2017**, *7*, 5773−5780.
(15) Kilburn, L.; DeLuca, M.; Hoffman, A. J.; Patel, S.; Hibbitts, D. Comparing Alkene-Mediated and Formaldehyde-Mediated Diene Formation Routes in Methanol-to-Olefins Catalysis in MFI and CHA. *J. Catal.* **2021**, *400*, 124−139.
(16) Wang, C.; Chu, Y.; Xu, J.; Wang, Q.; Qi, G.; Gao, P.; Zhou, X.; Deng, F. Extra-Framework Aluminum-Assisted Initial C−C Bond Formation in Methanol-to-Olefins Conversion on Zeolite H-ZSM-5. *Angew. Chem., Int. Ed.* **2018**, *57*, 10197−10201.
(17) Cesarini, A.; Mitchell, S.; Zichittella, G.; Agrachev, M.; Schmid, S. P.; Jeschke, G.; Pan, Z.; Bodi, A.; Hemberger, P.; Pérez-Ramírez, J. Elucidation of Radical- and Oxygenate-Driven Paths in Zeolite-Catalysed Conversion of Methanol and Methyl Chloride to Hydrocarbons. *Nat. Catal.* **2022**, *5*, 605−614.
(18) Hwang, A.; Kumar, M.; Rimer, J. D.; Bhan, A. Implications of Methanol Disproportionation on Catalyst Lifetime for Methanol-to-Olefins Conversion by HSSZ-13. *J. Catal.* **2017**, *346*, 154−160.
(19) Liu, Y.; Müller, S.; Berger, D.; Jelic, J.; Reuter, K.; Tonigold, M.; Sanchez-Sanchez, M.; Lercher, J. A. Formation Mechanism of the First Carbon-Carbon Bond and the First Olefin in the Methanol Conversion into Hydrocarbons. *Angew. Chem., Int. Ed.* **2016**, *55*, 5723−5726.
(20) Martinez-Espin, J. S.; De Wispelaere, K.; Westgård Erichsen, M.; Svelle, S.; Janssens, T. V. W.; Van Speybroeck, V.; Beato, P.; Olsbye, U. Benzene Co-Reaction with Methanol and Dimethyl Ether over Zeolite and Zeotype Catalysts: Evidence of Parallel Reaction Paths to Toluene and Diphenylmethane. *J. Catal.* **2017**, *349*, 136−148.
(21) Liu, Y.; Kirchberger, F. M.; Müller, S.; Eder, M.; Tonigold, M.; Sanchez-Sanchez, M.; Lercher, J. A. Critical Role of Formaldehyde during Methanol Conversion to Hydrocarbons. *Nat. Commun.* **2019**, *10*, 1462.
(22) Ni, Y.; Zhu, W.; Liu, Z. H-ZSM-5-Catalyzed Hydroacylation Involved in the Coupling of Methanol and Formaldehyde to Aromatics. *ACS Catal.* **2019**, *9*, 11398−11403.
(23) Hwang, A.; Bhan, A. Bifunctional Strategy Coupling Y_2O_3-Catalyzed Alkanal Decomposition with Methanol-to-Olefins Catalysis for Enhanced Lifetime. *ACS Catal.* **2017**, *7*, 4417−4422.
(24) Arora, S. S.; Shi, Z.; Bhan, A. Mechanistic Basis for Effects of High-Pressure H_2 Cofeeds on Methanol-to-Hydrocarbons Catalysis over Zeolites. *ACS Catal.* **2019**, *9*, 6407−6414.
(25) Wen, W.; Yu, S.; Zhou, C.; Ma, H.; Zhou, Z.; Cao, C.; Yang, J.; Xu, M.; Qi, F.; Zhang, G.; Pan, Y. Formation and Fate of Formaldehyde in Methanol-to-Hydrocarbon Reaction: In Situ Synchrotron Radiation Photoionization Mass Spectrometry Study. *Angew. Chem., Int. Ed.* **2020**, *59*, 4873−4878.
(26) Kirchberger, F. M.; Liu, Y.; Plessow, P. N.; Tonigold, M.; Studt, F. Mechanistic Differences between Methanol and Dimethyl Ether in Zeolite-Catalyzed Hydrocarbon Synthesis. *Proc. Natl. Acad. Sci. U. S. A.* **2022**, *119*, No. e2103840119.
(27) Kramer, Z. C.; Gu, X. K.; Zhou, D. D. Y.; Li, W. X.; Skodje, R. T. Following Molecules through Reactive Networks: Surface Catalyzed Decomposition of Methanol on Pd(111), Pt(111), and Ni(111). *J. Phys. Chem. C* **2014**, *118*, 12364−12383.
(28) Du, P.; Wu, P.; Cai, C. Mechanism of Methanol Decomposition on the $Pt_3Ni(111)$ Surface: DFT Study. *J. Phys. Chem. C* **2017**, *121*, 9348−9360.
(29) Xue, Z. H.; Han, J. T.; Feng, W. J.; Yu, Q. Y.; Li, X. H.; Antonietti, M.; Chen, J. S. Tuning the Adsorption Energy of Methanol Molecules Along Ni-N-Doped Carbon Phase Boundaries by the Mott−Schottky Effect for Gas-Phase Methanol Dehydrogenation. *Angew. Chem., Int. Ed.* **2018**, *57*, 2697−2701.
(30) Zhang, Z.; Su, J.; Matias, A. S.; Gordon, M.; Liu, Y. S.; Guo, J.; Song, C.; Dun, C.; Prendergast, D.; Somorjai, G. A.; Urban, J. J. Enhanced and Stabilized Hydrogen Production from Methanol by Ultrasmall Ni Nanoclusters Immobilized on Defect-Rich h-BN Nanosheets. *Proc. Natl. Acad. Sci. U. S. A.* **2020**, *117*, 29442−29452.
(31) Li, Z.; Potapenko, D. V.; Rim, K. T.; Flytzani-Stephanopoulos, M.; Flynn, G. W.; Osgood, R. M.; Wen, X. D.; Batista, E. R. Reactions of Deuterated Methanol (CD_3OD) on $Fe_3O_4(111)$. *J. Phys. Chem. C* **2015**, *119*, 1113−1120.
(32) Gamba, O.; Hulva, J.; Pavelec, J.; Bliem, R.; Schmid, M.; Diebold, U.; Parkinson, G. S. The Role of Surface Defects in the Adsorption of Methanol on $Fe_3O_4(001)$. *Top. Catal.* **2017**, *60*, 420−430.
(33) Ortega, J. M.; Gayubo, A. G.; Aguayo, A. T.; Olazar, M.; Bilbao, J. MTG Process in a Fluidized Bed with Catalyst Circulation: Operation and Simulation of an Experimental Unit. *Ind. Eng. Chem. Res.* **1998**, *37*, 4222−4230.
(34) Bozzano, A. G.; Bradley, S. A.; Castillo, R. L.; Chen, J. Q. Methanol-to-olefins process with reduced coking. US Patent, 7,763,766, 2010.
(35) Dojahn, J. G.; Wentworth, W. E.; Stearns, S. D. Characterization of Formaldehyde by Gas Chromatography Using Multiple Pulsed-Discharge Photoionization Detectors and a Flame Ionization Detector. *J. Chromatogr. Sci.* **2001**, *39*, 54−58.
(36) Zanchet, A.; García, G. A.; Nahon, L.; Bañares, L.; Marggi Poullain, S. Signature of a Conical Intersection in the Dissociative

https://doi.org/10.1021/acscatal.2c02953
ACS Catal. 2022, 12, 13426−13434

Photoionization of Formaldehyde. *Phys. Chem. Chem. Phys.* **2020**, *22*, 12886−12893.
(37) Nach, T. The Colorimetric Estimation of Formaldehyde by Means of the Hantzsch Reaction. *Biochem. J.* **1953**, *55*, 416−421.
(38) Sztáray, B.; Voronova, K.; Torma, K. G.; Covert, K. J.; Bodi, A.; Hemberger, P.; Gerber, T.; Osborn, D. L. CRF-PEPICO: Double Velocity Map Imaging Photoelectron Photoion Coincidence Spectroscopy for Reaction Kinetics Studies. *J. Chem. Phys.* **2017**, *147*, 13944−13954.
(39) Hemberger, P.; Custodis, V. B. F.; Bodi, A.; Gerber, T.; van Bokhoven, J. A. Understanding the Mechanism of Catalytic Fast Pyrolysis by Unveiling Reactive Intermediates in Heterogeneous Catalysis. *Nat. Commun.* **2017**, *8*, 15946.
(40) Hemberger, P.; Van Bokhoven, J. A.; Pérez-Ramírez, J.; Bodi, A. New Analytical Tools for Advanced Mechanistic Studies in Catalysis: Photoionization and Photoelectron Photoion Coincidence Spectroscopy. *Catal. Sci. Technol.* **2020**, *10*, 1975−1990.
(41) Puente-Urbina, A.; Pan, Z.; Paunović, V.; Hemberger, P.; Bokhoven, J. A. Direct Evidence on the Mechanism of Methane Conversion under Non-Oxidative Conditions over Iron-Modified Silica: The Role of Propargyl Radicals Unveiled. *Angew. Chem., Int. Ed.* **2021**, *60*, 24002−24007.
(42) Bodi, A.; Sztáray, B.; Baer, T.; Johnson, M.; Gerber, T. Data Acquisition Schemes for Continuous Two-Particle Time-of-Flight Coincidence Experiments. *Rev. Sci. Instrum.* **2007**, *78*, No. 084102.
(43) Osborn, D. L.; Hayden, C. C.; Hemberger, P.; Bodi, A.; Voronova, K.; Sztáray, B. Breaking through the False Coincidence Barrier in Electron-Ion Coincidence Experiments. *J. Chem. Phys.* **2016**, *145*, 164202.
(44) Bodi, A.; Johnson, M.; Gerber, T.; Gengeliczki, Z.; Sztáray, B.; Baer, T. Imaging Photoelectron Photoion Coincidence Spectroscopy with Velocity Focusing Electron Optics. *Rev. Sci. Instrum.* **2009**, *80*, No. 034101.
(45) Takeshita, K. A Theoretical Study on the Ionic States, with Analysis of Vibrational Levels of the Photoelectron Spectrum, of Formic Acid (CH_2O_2 and CD_2O_2). *Chem. Phys.* **1991**, *94*, 7259−7269.
(46) Biesinger, M. C.; Payne, B. P.; Grosvenor, A. P.; Lau, L. W. M.; Gerson, A. R.; Smart, R. S. C. Resolving Surface Chemical States in XPS Analysis of First Row Transition Metals, Oxides and Hydroxides: Cr, Mn, Fe, Co and Ni. *Appl. Surf. Sci.* **2011**, *257*, 2717−2730.
(47) Xie, J.; Firth, D. S.; Cordero-Lanzac, T.; Airi, A.; Negri, C.; Øien-Ødegaard, S.; Lillerud, K. P.; Bordiga, S.; Olsbye, U. MAPO-18 Catalysts for the Methanol to Olefins Process: Influence of Catalyst Acidity in a High-Pressure Syngas (CO and H_2) Environment. *ACS Catal.* **2022**, *12*, 1520−1531.

https://doi.org/10.1021/acscatal.2c02953
ACS Catal. 2022, 12, 13426−13434